Size-Dependent Flexural Dynamics of Ribs-Connected Polymeric Micropanels

K.B. Mustapha[1,2]

Abstract: This study investigates the sensitivity of the flexural response of a rib-connected system of coupled micro-panels with traction-free surfaces. Idealized as a two-dimensional elastic continuum with a finite transverse stiffness, each micro-panels' behavior is examined within the framework of the biharmonic mathematical model derived from the higher-order, size-dependent strain energy formulation. The model incorporates the material length scale, which bears an associative relationship with the underlying polymer's averaged Frank elastic constant. Upper estimates of the eigenvalue of the system, under fully clamped edges and simply-supported edges, are determined by the Rayleigh method. The adopted theory for the micro-panel's behavior takes into account the rotary inertia, the small-scale effect, the Poisson's ratio and the effective stiffness of the ribs, but neglects shear distortion. Frequency shifts of the rib-connected coupled micro-panels are systematically identified and presented. Results indicate the critical thickness for which the polymeric micro-panel's resonant frequency starts to experience stiffened responses based on the magnitude of the size-effect. The Rayleigh method of eigenvalue extraction is augmented with the applied statistical method of design of experiment for the discovery of notable interaction effects between the aspect ratio, rotary inertia, small-scale effect, and thickness-to-span ratio of the system.

Keywords: Modified couple stress, Micro plates, Size-effect, Vibration, Rayleigh method.

1   Introduction

Microelectromechanical and nanoelectromechanical systems (MEMs and NEMS) occupy preeminent functional roles within the landscape of next generation devices. Often endowed with micro-sized structures, MEMs and NEMs have found unal-

---

[1] Faculty of Engineering, Computing and Science, Swinburne University of Technology (Sarawak Campus), Jalan Simpang Tiga, Kuching 93350, Sarawak, Malaysia.
[2] Corresponding author. Tel: +6082260656; E-mail: kbmustapha@swinburne.edu.my

loyed advantage in portable field accelerometers, electrical filters, hydrophones, high-Q oscillators and inertia sensors [Nguyen (1995); Yazdi, Ayazi and Najafi (1998); Kun and Nguyen (1999); Mattila, Kiihamäki, Lamminmäki, Jaakkola, Rantakari, Oja, Seppä, Kattelus and Tittonen (2002)]. A number of reasons shape the adoption of micro-systems across different emerging scientific fields: (i) prodigious capacity for fast response; (ii) ultra-high resonating frequency; and (iii) a high sensitivity to changes in stimulus.

The complexity of most microsystems depends on the intended functional purpose and operational requirements. In a simple form, a microsystem comprises cantilever arrays along with some other functional embodiment. In a more complex form, however, it may be composed of structural elements with different geometrical parameters for different functional purposes [Boisen, Dohn, Keller, Schmid and Tenje (2011)]. Among the unique set of structural elements routinely employed in MEMs is the two-dimensional plate-like micro-scale structures (e.g. thin film, micro-scale panels, and orthotropic micron metallic web [Benkhelifa, Farnsworth, Tiwari and Bandi (2010)]. These micro-structural elements have excellent magnetic, optical, mechanical and electrical properties that make them resourceful in specific applications like thermal sealing and energy harvesting [Sakhaee-Pour, Ahmadian and Vafai (2008); Liu, Tu and Chung (2012); Manzaneque, Ruiz, Hernando-Garcia, Ababneh, Seidel and Sanchez-Rojas (2012)] Since the optimal design of MEMs and NEMs impels the understanding of their response under disparate mechanical loadings, the analyses of their constituent micro-structural elements has gained attention in the past few years [Younis (2011)]. During the operational life of MEMs, some factors compromise the exhibition of their intended performance [Ardito, Baldasarre, Corigliano, De Masi, Frangi and Magagnin (2013)]. Frequently, such factors are closely related to the inter-relationship between the mechanical parameters of the underlying materials and the geometric parameters of the system's architecture. This interplay imposes a strict constrain on the predictability of MEMs' mechanical responses.

Several studies relating to the prediction of MEMs' response have revealed the demands for the refinement of the mathematical models of the constituent elements of these miniature devices [Peddieson, Buchanan and McNitt (2003); Reddy (2011); Mustapha (2014)]. This is because, at small length scale, the vexing contribution of size-effect to the response of the structures starts to set in. Initial studies on the modeling of micro-scale structures through the framework of computational mechanics, employed the classical continuum theory (CCT). However, the underlying assumptions of the CCT do not account for the contribution of the latent size-dependency that manifests in micro and nano-scale structures [Fleck and Hutchinson (1993); Georgiadis and Velgaki (2003); Liew, Wong, He, Tan and Meguid

(2004); Uchic, Dimiduk, Florando and Nix (2004); Volkert and Lilleodden 2006; Mahdavi, Farshidianfar, Tahani, Mahdavi and Dalir (2008); Chiroiu, Munteanu and Delsanto (2010)]. It is this deficiency of the CCT that has ignited the adoption of a number of enriched microstructure-dependent elasticity theories with higher-order constitutive laws [Farokhi, Ghayesh and Amabili (2013)]. The models derived from these higher-order theories contain additional material constants, along with the well-known Lamé constants, to address the quantification of the phenomenological size-specific property.

Evidently, attempt on the theoretical modeling of microstructured materials stretches back to the work of the Cosserat brothers [Cosserat E. and F (1909); Chiroiu, Munteanu and Gliozzi (2010)]. Consolidating on the work of the Cosserat brothers, a select list of advanced continuum theories that have emerged to be of relevant to the modeling of microstructured materials include the Eringen's nonlocal elasticity theory [Eringen (1972); Eringen and Edelen (1972); Fotouhi, Firouz-Abadi and Haddadpour (2013)], the strain gradient theory [Aifantis (1992); Tang, Shen and Atluri (2003); Papacharalampopoulos, Karlis, Charalambopoulos and Polyzos (2010)], the couple stress theory [Toupin (1962); Yang, Chong, Lam and Tong (2002)] and the micropolar elasticity [Toupin (1962); Xie and Long (2006); Marin, Agarwal and Othman (2014)]. A concise summary of the distinction between these theories is well-stated in Aifantis [Aifantis (2011)]. Meanwhile, a well-founded challenge with the new higher-order models is the difficulty associated with the determination of the microstructure-dependent material constants introduced by these theories [Lam, Yang, Chong, Wang and Tong (2003)]. Consequently, models of the structural elements with fewer length scale parameters offer both experimental benefit and mathematical convenience. The modified couple stress theory (MCST), which is adopted in the current study, is one such higher-order elasticity theories. With the MCST, the characterization of size-effect is done with just one material length scale parameter [Yang, Chong, Lam and Tong (2002); Papargyri-Beskou, Tsepoura, Polyzos and Beskos (2003)]. The MCST has already set off a burst of research activities in the theoretical prediction of the deformational response of micro-scale structural elements. Initial application of the MCST focused on the analyses of micro-scale beams, rods and micro-scale pipes [Anthoine (2000); Park and Gao (2006); Güven (2011); Reddy (2011); Mustapha and Zhong (2012); Mustapha and Zhong (2012); Akgöz and Civalek (2013); Wang, Liu, Ni and Wu (2013)]. However, a limited number of recent studies have also extended the work to the analyses of micro-scale plates [Yin, Qian, Wang and Xia (2010); Jomehzadeh, Noori and Saidi (2011); Akgöz and Civalek (2013); Gao, Huang and Reddy (2013)] An experimental validation of the MCST is recently presented in Romanoff and Reddy (2014).

Drawing on the strength of the MCST, the present study investigates the size-dependent flexural vibration of a rib-connected system of micro-panels. The system under investigation is part of an on-going design of a polymeric vibration isolation pad for electronic communicating systems. For the derivation, each micro-panel is treated as a micro-scale plate with an internal material length scale. The stiffness of the ribs between the micro-panel is derived by treating the ribs as a collection of clamped-clamped elastic beams. A hybrid numerical experiment based on the Rayleigh method of eigenvalue extraction and an applied statistical method of design of experiment (DOE) is adopted for parametric analysis of the derived model. The adopted hybrid approach helps to illuminate the pattern of the resonant frequency shifts under varying influences of the stiffness of the ribs. The effects of the material length scale of the micro-panel, the Poisson's ratio and the rotary inertia are also assessed. The ensuing part of the paper proceeds with the presentation of the derivation of the size-dependent elastodynamics governing equation of the system in section 2. The solution procedure for the free vibration study is detailed in section 3. Reduced special cases of the derived model are highlighted in section 4. In section 5, numerical results and the discussion of the influence of the model's parameters on the frequency shift of the system are presented. Basic conclusions from the analysis are given in section 6.

2   Variational Formulation

2.1   The higher-order elasticity theory

The system being considered is the elastically connected micro-panels shown in Fig. 1. In what follows, the equations governing the flexural vibration of each micro-panel are derived from the Hamilton's principle and the modified couple stress theory (MCST). In deriving the governing equation, we treat each micro-panel as an isotropic linear elastic body occupying a volume $\forall$. In line with the theoretical framework of the MCST, the size-dependent strain energy of a deformed micro-scale structure is characterized by a quartet of tensors related as [Yang, Chong, Lam and Tong (2002); Reddy (2011)]:

$$\Pi_U = \frac{1}{2} \int_{\forall} (\boldsymbol{\sigma} : \boldsymbol{\varepsilon} + \boldsymbol{m} : \boldsymbol{\chi}) \, d\forall. \tag{1}$$

In general, the volume $\forall$ is taken to be an open set in R^3 with a well-behaved surface boundary (see Fig. 1b for the unit normal to the boundaries' of a micro-panel). Accordingly, Π_U, $\boldsymbol{\varepsilon}$ and $\boldsymbol{\sigma}$ are the strain energy, the dilatation strain tensor and the Cauchy stress tensor, respectively. Furthermore, the tensors $\boldsymbol{m}$ and $\boldsymbol{\chi}$ refer to the deviatoric components of the couple stress and the symmetric curvature tensor, respectively.
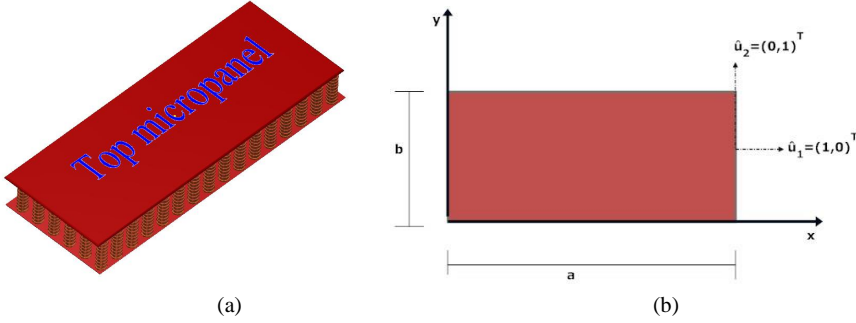
(a) (b)

Figure 1: Schematic of the rib-connected system of micro-panels: (a) a 3D view of the coupled system; and (b) the mid-plane of a micro-panel with the adopted coordinate system.

Given that the deformation of a material point of the micro-panel is described by the displacement field $\boldsymbol{u}$ and a rotation vector $\boldsymbol{\theta}$, then the tensors $\boldsymbol{\varepsilon}$ and $\boldsymbol{\chi}$ in Eq. (1) are known to satisfy the following geometric relations:

$$\boldsymbol{\varepsilon} = \frac{1}{2}\left[\nabla\boldsymbol{u} + (\nabla\boldsymbol{u})^T\right] \tag{2}$$

$$\boldsymbol{\chi} = \frac{1}{2}\left[\nabla\boldsymbol{\theta} + (\nabla\boldsymbol{\theta})^T\right] \tag{3}$$

where the operator ∇ is the 2D gradient notation. From kinematics consideration, the rotation vector $\boldsymbol{\theta}$ is easily related to the displacement field in the form:

$$\boldsymbol{\theta} = \frac{1}{2}\text{curl } \boldsymbol{u} \tag{4}$$

Additionally, the stress fields ($\boldsymbol{\sigma}$ and $\boldsymbol{m}$) are mapped to the displacement field through the enriched constitutive rules as:

$$\boldsymbol{\sigma} = \lambda\,\text{tr}(\varepsilon)\,\mathbf{I} + 2G\varepsilon \tag{5a}$$

$$\boldsymbol{m} = 2\zeta^2\mu\boldsymbol{\chi} \tag{5b}$$

In Eq. (5a) the stress field is related to the displacement field through the parameters λ (the bulk modulus) and G (the shear modulus) respectively. However, in Eq. (5b), the higher-order stress field ($\boldsymbol{m}$) is related to the displacement field through an additional material constant (ζ) This new constant is associated with the material length scale parameter [Reddy (2011)].

For the purpose of characterizing the deformation of the micro-panel through the above higher-order constitutive rules, an infinitesimal bounded volume of the micro-panel is considered. The infinitesimal bounded volume of the micro-panel is treated as a differentiable manifold embedded in a Euclidean 3-space $\forall$. Consequently, the following displacement trial field holds:

$$\boldsymbol{u} = u_1\boldsymbol{i} + u_2\boldsymbol{j} + u_3\boldsymbol{k} \tag{6}$$

where u_1, u_2, and u_3 are components of the displacement vector of an arbitrary material point of the micro-panel in the x, y and z directions. Based on the small-deflection theory of thin plates, which rests on the Kirchhoff assumptions, each of these components of the displacement field is defined as:

$$u_1(x,y,z,t) = u(x,y,t) - z\frac{\partial w(x,y,t)}{\partial x} \tag{7a}$$

$$u_2(x,y,z,t) = v(x,y,t) - z\frac{\partial w(x,y,t)}{\partial y} \tag{7b}$$

$$u_3(x,y,z,t) = w(x,y,t) \tag{7c}$$

where u, v, and w are displacement components in the x, y and z directions, respectively. Based on Eqs. (7a) – (7c), the non-zero components of the strain tensor are obtained as:

$$\varepsilon_{xx} = \frac{\partial u}{\partial x} - z\frac{\partial^2 w}{\partial x^2} \tag{8a}$$

$$\varepsilon_{yy} = \frac{\partial v}{\partial y} - z\frac{\partial^2 w}{\partial y^2} \tag{8b}$$

$$\varepsilon_{xy} = \varepsilon_{yx} = \frac{1}{2}\left[\frac{\partial u}{\partial y} + \frac{\partial v}{\partial x} - 2z\frac{\partial^2 w}{\partial y\partial x}\right] \tag{8c}$$

The components of the rotation vector, from Eq. (4), are obtained as:

$$\theta_x = \frac{\partial w}{\partial x}; \quad \theta_y = -\frac{\partial w}{\partial y}; \quad \theta_z = \frac{1}{2}\left[-\frac{\partial u}{\partial y} + \frac{\partial v}{\partial x}\right] \tag{9}$$

With the help of Eq. (9) bearing in mind Eq. (3), the components of the symmetric curvature tensor, are derived as:

$$\chi_{xx} = \frac{\partial^2 w}{\partial y\partial x}; \quad \chi_{yy} = -\frac{\partial^2 w}{\partial y\partial x}; \quad \chi_{zz} = 0 \tag{10a}$$

$$\chi_{xy} = \chi_{yx} = \frac{1}{2}\left[-\frac{\partial^2 w}{\partial x^2} + \frac{\partial^2 w}{\partial y^2}\right] \tag{10b}$$

$$\chi_{zy} = \chi_{yz} = \frac{1}{4}\left[-\frac{\partial^2 u}{\partial y \partial x} + \frac{\partial^2 v}{\partial x^2}\right] \tag{10c}$$

$$\chi_{zx} = \chi_{xz} = \frac{1}{4}\left[-\frac{\partial^2 u}{\partial y^2} + \frac{\partial^2 v}{\partial y \partial x}\right] \tag{10d}$$

Given the above derived kinematic variables, the first variation of the microstructure-dependent strain energy is now written as:

$$\delta\Pi_U = \frac{1}{2}\delta\int\int\int_{-h/2}^{h/2}\left[\frac{E}{(1-v^2)}\varepsilon_{xx}^2 + \frac{E}{(1-v^2)}\varepsilon_{yy}^2 + \frac{2vE}{(1-v^2)}\varepsilon_{yy}\varepsilon_{xx} + G\varepsilon_{yx}^2 + \right.$$

$$\left. G\{\zeta^2\mu(\chi_{xx})^2 + \zeta^2\mu(\chi_{yy})^2 + \zeta^2\mu(2\chi_{xy})^2 + \zeta^2\mu(2\chi_{yz})^2 + \zeta^2\mu(2\chi_{xz})^2\}\right]dxdydz \tag{11}$$

From the displacement field defined in Eq. (7), the first variation of the kinetic energy, with the rotary inertia included, is defined as [Reddy (2002); Szilard (2004)]:

$$\delta\Pi_T = \frac{1}{2}\delta\int\int\rho h\left[\left(\frac{\partial u_1}{\partial t}\right)^2 + \left(\frac{\partial u_2}{\partial t}\right)^2 + \left(\frac{\partial u_3}{\partial t}\right)^2\right]dydx \tag{12}$$

where ρ is the mass density and h is the constant thickness of the micro-panel. In the same spirit, the first variation of the virtual work done by external loads is [Akgöz and Civalek (2013)]:

$$\int_0^T \delta\Pi_{WB} = -\int_R (f_i\delta u_i + c_i\delta\theta_i) - \int_{\partial R}(t_i\delta u_i + s_i\delta\theta_i)\,ds \tag{13}$$

where f_i, c_i, t_i and s_i are components of the body force, the body couple, the traction and the surface couple, respectively. With Eqs. (11) – (13), one invokes the variational statement of the Hamilton's principle, which mathematically translates to:

$$\delta\int_0^T (\Pi_T - \Pi_U + \Pi_{WB})\,dt = 0 \tag{14}$$

where the integration in Eq. (14) is carried out between the time interval $(0,T)$. Eqs. (11) – (13) are substituted in Eq. (14), and the fundamental lemma of variational calculus is invoked to retrieve the size-dependent governing equations of a single micro-panel as:

$$-\rho h\frac{\partial^2 u}{\partial t^2} + Eh\left[\frac{1}{2(1+v)}\frac{\partial^2 u}{\partial y^2} + \frac{1}{2(1-v)}\frac{\partial^2 v}{\partial y \partial x} + \frac{1}{1-v^2}\frac{\partial^2 u}{\partial x^2}\right]$$

$$+\frac{Eh\zeta^2}{8(1+v)}\left[\frac{\partial^4 v}{\partial y^3 \partial x} - \frac{\partial^4 u}{\partial y^4} - \frac{\partial^4 u}{\partial x^2 \partial y^2} + \frac{\partial^4 v}{\partial x^3 \partial y}\right] = 0 \tag{15}$$

$$-\rho h \frac{\partial^2 v}{\partial t^2} + Eh \left[\frac{1}{1-v^2} \frac{\partial^2 v}{\partial y^2} + \frac{1}{2(1-v)} \frac{\partial^2 u}{\partial y \partial x} + \frac{1}{2(1+v)} \frac{\partial^2 v}{\partial x^2} \right]$$
$$+ \frac{Eh\zeta^2}{8(1+v)} \left[\frac{\partial^4 u}{\partial y^3 \partial x} - \frac{\partial^4 v}{\partial x^2 \partial y^2} + \frac{\partial^4 u}{\partial x^3 \partial y} + \frac{\partial^4 v}{\partial x^4} \right] = 0 \tag{16}$$

$$-\rho h \frac{\partial^2 w}{\partial t^2} + \rho I \left[\frac{\partial^4 w}{\partial t^2 \partial y^2} + \frac{\partial^4 w}{\partial t^2 \partial x^2} \right] - \frac{Eh^3}{12(1-v^2)} \left[\frac{\partial^4 w}{\partial y^4} + 2\frac{\partial^4 w}{\partial x^2 \partial y^2} + \frac{\partial^4 w}{\partial x^4} \right]$$
$$- \frac{Eh\zeta^2}{2(1+v)} \left[\frac{\partial^4 w}{\partial y^4} + 2\frac{\partial^4 w}{\partial x^2 \partial y^2} + \frac{\partial^4 w}{\partial x^4} \right] = 0 \tag{17}$$

The terms that arise from the use of the MCST are underlined in Eqs. (15) – (17). In general, Eqs. (15) and (16) are adequate to predict the in-plane (extensional) vibration of a single micro-panel. On the other hand, Eq. (17) is suitable for the quantification of the transverse motion of a single micro-panel. Now, while Eq. (17) can be tackled alone, Eqs. (15) and (16) are coupled, and thus they cannot be solved independent of each other. Of interest in this study is the case of two inextensible micro-panels separated by evenly distributed ribs. On this premise, the focus of the current study is restricted to Eq(17) and its eigen-analysis. For the purpose of incorporating the influence of the ribs, the following assumptions are adopted:

1. the ribs are made of similar materials and have resistance to stretching and compression;

2. the ribs suffer negligibly marginal distortion of their positions with respect to their initial contact positions with the surface of each micro-panel;

3. no structural anisotropy is introduced by the ribs and;

4. the two micro-panels are made of the same material, length, width and density.

With the stated assumptions, the concentrated rigidities of the ribs can be replaced by the distributed continuous support of the Winkler's type. Given this simplification, the contribution of the ribs' stiffness is now reflected in the equation governing the transverse vibration of individual micro-panel as:

Upper micro-panel:

$$-\rho h \frac{\partial^2 w_u}{\partial t^2} + \rho I \left[\frac{\partial^4 w_u}{\partial t^2 \partial y^2} + \frac{\partial^4 w_u}{\partial t^2 \partial x^2} \right] - \frac{Eh^3}{12\left(1 - v^2\right)} \left[\frac{\partial^4 w_u}{\partial y^4} + 2\frac{\partial^4 w_u}{\partial x^2 \partial y^2} + \frac{\partial^4 w_u}{\partial x^4} \right]$$

$$- \frac{Eh\zeta^2}{2\left(1 + v\right)} \left[\frac{\partial^4 w_u}{\partial y^4} + 2\frac{\partial^4 w_u}{\partial x^2 \partial y^2} + \frac{\partial^4 w_u}{\partial x^4} \right] - K\left(w_u - w_l\right) = 0$$

(18)

Lower micro-panel:

$$-\rho h \frac{\partial^2 w_l}{\partial t^2} + \rho I \left[\frac{\partial^4 w_l}{\partial t^2 \partial y^2} + \frac{\partial^4 w_l}{\partial t^2 \partial x^2} \right] - \frac{Eh^3}{12\left(1 - v^2\right)} \left[\frac{\partial^4 w_l}{\partial y^4} + 2\frac{\partial^4 w_l}{\partial x^2 \partial y^2} + \frac{\partial^4 w_l}{\partial x^4} \right]$$

$$- \frac{Eh\zeta^2}{2\left(1 + v\right)} \left[\frac{\partial^4 w_l}{\partial y^4} + 2\frac{\partial^4 w_l}{\partial x^2 \partial y^2} + \frac{\partial^4 w_l}{\partial x^4} \right] - K\left(w_l - w_u\right) = 0$$

(19)

It is pointed out that in Eqs. (18) – (19), the total stiffness (K) of the Winkler's foundation is taken to be equivalent to the averaged stiffness of the overall ribs between the micro-panels. Besides, w_u and w_l denote the transverse motions of the upper and lower micro-panel, respectively. The two displacement field variables describing the response of each micro-panel are homogenized by subtracting Eq. (19) from (18) to get:

$$-\rho h \frac{\partial^2 \left(w_u - w_l\right)}{\partial t^2} + \rho I \left[\frac{\partial^4}{\partial t^2 \partial y^2} + \frac{\partial^4}{\partial t^2 \partial x^2} \right] \left(w_u - w_l\right)$$

$$- \frac{Eh^3}{12\left(1 - v^2\right)} \left[\frac{\partial^4}{\partial y^4} + 2\frac{\partial^4}{\partial x^2 \partial y^2} + \frac{\partial^4}{\partial x^4} \right] \left(w_u - w_l\right)$$

(20)

$$- \frac{Eh\zeta^2}{2\left(1 + v\right)} \left[\frac{\partial^4}{\partial y^4} + 2\frac{\partial^4}{\partial x^2 \partial y^2} + \frac{\partial^4}{\partial x^4} \right] \left(w_u - w_l\right) - 2K\left(w_u - w_l\right) = 0$$

A further modification of the system's response is sought by employing a change of variable as done in Murmu and Adhikari (2011). In this vein, the relative displacement $(w_u - w_l)$ of the upper micro-panel with respect to the lower micro-panel is denoted by w_a. The change of variable leads to the equations of the rib-connected micro-panels as:

$$-\rho h \frac{\partial^2 w_a}{\partial t^2} + \rho I \left[\frac{\partial^4}{\partial t^2 \partial y^2} + \frac{\partial^4}{\partial t^2 \partial x^2} \right] w_a$$

$$- \frac{Eh^3}{12\left(1 - v^2\right)} \left[\frac{\partial^4}{\partial y^4} + 2\frac{\partial^4}{\partial x^2 \partial y^2} + \frac{\partial^4}{\partial x^4} \right] w_a$$

(21)

$$- \frac{Eh\zeta^2}{2\left(1 + v\right)} \left[\frac{\partial^4}{\partial y^4} + 2\frac{\partial^4}{\partial x^2 \partial y^2} + \frac{\partial^4}{\partial x^4} \right] w_a - 2Kw_a = 0$$

$$-\rho h\frac{\partial^2 w_l}{\partial t^2}+\rho I\left[\frac{\partial^4 w_l}{\partial t^2\partial y^2}+\frac{\partial^4 w_l}{\partial t^2\partial x^2}\right]w_a-\frac{Eh^3}{12\left(1-v^2\right)}\left[\frac{\partial^4 w_l}{\partial y^4}+2\frac{\partial^4 w_l}{\partial x^2\partial y^2}+\frac{\partial^4 w_l}{\partial x^4}\right]$$

$$-\frac{Eh\zeta^2}{2\left(1+v\right)}\left[\frac{\partial^4 w_l}{\partial y^4}+2\frac{\partial^4 w_l}{\partial x^2\partial y^2}+\frac{\partial^4 w_l}{\partial x^4}\right]+Kw_a=0$$

$$(22)$$

Equations (21) and (22) describe the transverse motion of the connected micro-panels, where I is the moment of inertia per unit area of a micro-panel. It deserves to be pointed out that if the underlined terms are eliminated, the classical size-independent governing equation of the Kirchhoff plate theory is retrieved. In succeeding sections, the dynamic behavior of the system is investigated under two idealized boundary conditions: (i) simple support on the four edges (that is, SSSS, where S stands for simply-supported); and (ii) a built-in support on the four edges (that is, CCCC, where C stands for clamped) as shown in Fig. 2.
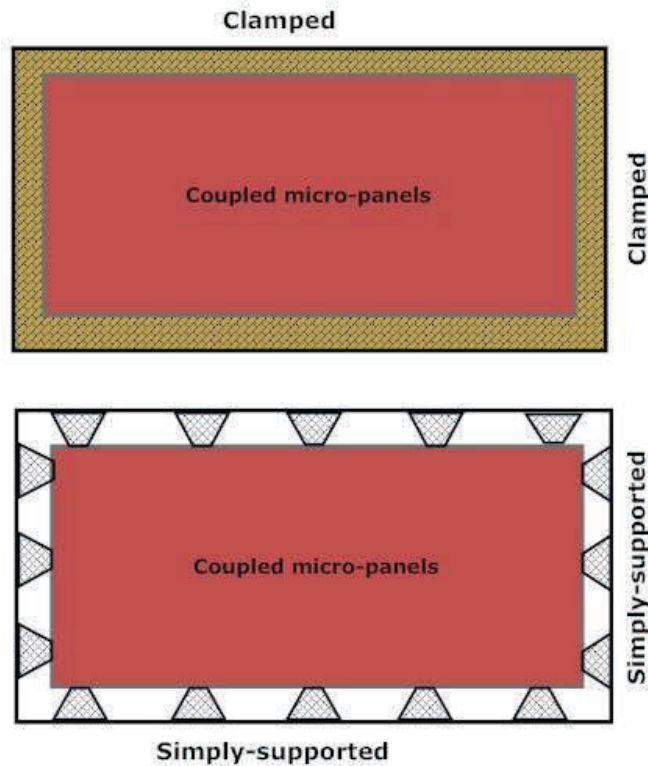

Figure 2: The two types of boundary supports investigated for the rib-connected micro-panels.

In order to specify the expressions for the stipulated boundary conditions the following stress resultants are defined:

$$\begin{Bmatrix} C_{xx} \\ C_{xy} \\ C_{xz} \\ C_{yy} \\ C_{yz} \end{Bmatrix} = \int_{-h/2}^{h/2} \begin{Bmatrix} m_{xx} \\ m_{xy} \\ m_{xz} \\ m_{yy} \\ m_{yz} \end{Bmatrix} dz \tag{23}$$

$$\begin{Bmatrix} M_{xx} \\ M_{xy} \\ M_{yy} \end{Bmatrix} = \int_{-h/2}^{h/2} \begin{Bmatrix} \sigma_{xx} \\ \sigma_{xy} \\ \sigma_{yy} \end{Bmatrix} z dz \tag{24}$$

where $C_{xx}, C_{xy}, C_{xz} C_{yy}$ and C_{yz} are the couple moments that need to be mapped to the displacement field through Eq. (10). Also, $\boldsymbol{M}_{xx}, \boldsymbol{M}_{xy}$ and $\boldsymbol{M}_{yy}$ are the moments (related to the Cauchy stress tensor) that are mapped to the displacement field through Eq. (8). Under the SSSS boundary condition, the following constraints are imposed around the periphery of the coupled micro-panels:

$$w_a(0,y,t) = w_u(0,y,t) - w_l(0,y,t) = 0 \tag{25}$$

$$w_a(a,0,t) = w_u(a,0,t) - w_l(a,0,t) = 0 \tag{26}$$

$$w_a(x,0,t) = w_u(x,0,t) - w_l(x,0,t) = 0 \tag{27}$$

$$w_a(x,b,t) = w_u(x,b,t) - w_l(x,b,t) = 0 \tag{28}$$

$$M_{xxa}(0,y,t) + C_{xya}(0,y,t) = 0 \tag{29}$$

$$M_{xxa}(a,y,t) + C_{xya}(a,y,t) = 0 \tag{30}$$

$$-M_{yya}(x,0,t) + C_{xya}(x,0,t) = 0 \tag{31}$$

$$-M_{yya}(x,b,t) + C_{xya}(x,b,t) = 0 \tag{32}$$

Analogously, under the CCCC boundary condition the expressions stated in Eqs. (25) – (28), are supplemented with the following additional constraints around the periphery of coupled micro-panels:

$$\frac{\partial}{\partial x}w_a(0,y,t) = \frac{\partial}{\partial x}[w_u(0,y,t) - w_l(0,y,t)] = 0 \tag{33}$$

$$\frac{\partial}{\partial x}w_a(a,0,t) = \frac{\partial}{\partial x}[w_u(a,0,t) - w_l(a,0,t)] = 0 \tag{34}$$

$$\frac{\partial}{\partial x}w_a(x,0,t) = \frac{\partial}{\partial x}[w_u(x,0,t) - w_l(x,0,t)] = 0 \tag{35}$$

$$\frac{\partial}{\partial x}w_a(x,b,t) = \frac{\partial}{\partial x}[w_u(x,b,t) - w_l(x,b,t)] = 0 \tag{36}$$

3   Solution Procedure

The Rayleigh method is adopted to evaluate the dynamic response of the system. The energy functional Π from the governing equation of the coupled is defined as:

$$\Pi = [(\Pi_U)_{maxu} + (\Pi_U)_{maxl}] - [(\Pi_T)_{maxu} + (\Pi_T)_{maxl}] \tag{37}$$

where $(\Pi_U)_{maxu}$ and $(\Pi_U)_{maxl}$ represent the maximum strain energy of the upper and lower micro-panels, respectively. Equally, $(\Pi_T)_{maxu}$ and $(\Pi_T)_{maxl}$ represent the maximum kinetic energy of the upper and lower micro-panels, respectively. As it is often a good practice to cast the governing equation into the non-dimensional form, the following parameters are introduced:

$$\xi = x/a; \quad \eta = y/b; \quad \varphi = a/b; \quad D = \frac{Eh^3}{12\left(1 - \upsilon^2\right)} \tag{38}$$

With the non-dimensional parameters, the explicit expressions for the maximum energy terms for the overall system become:

$$
(\Pi_U)_{\max}
$$

$$
= \frac{1}{2} \int_0^1 \int_0^1 \left\{ D \left[\left(\frac{\partial^2 w_a}{\partial \xi^2} \right)^2 + \left(\frac{\partial^2 w_a}{\partial \eta^2} \right)^2 + 2\upsilon \frac{\partial^2 w_a}{\partial \xi^2} \frac{\partial^2 w_a}{\partial \eta^2} + (2 - \upsilon) \left(\frac{\partial^2 w_a}{\partial \left(1 + \upsilon \right)} \right)^2 \right] \right.
$$

$$
+ \frac{Eh\zeta^2}{2\left(1 + \upsilon\right)} \left[\left(\frac{\partial^2 w_a}{\partial \xi^2} \right)^2 + \left(\frac{\partial^2 w_a}{\partial \eta^2} \right)^2 + 2 \left(\frac{\partial^2 w_a}{\partial \xi \partial \eta} \right)^2 \right] + 2K w_a^2
$$

$$
+ D \left[\left(\frac{\partial^2 w_l}{\partial \xi^2} \right)^2 + \left(\frac{\partial^2 w_l}{\partial \eta^2} \right)^2 + 2\upsilon \frac{\partial^2 w_l}{\partial \xi^2} \frac{\partial^2 w_l}{\partial \eta^2} + (2 - \upsilon) \left(\frac{\partial^2 w_l}{\partial \xi \partial \eta} \right) \right]
$$

$$
\left. + \frac{Eh\zeta^2}{2\left(1 + \upsilon\right)} \left[\left(\frac{\partial^2 w_l}{\partial \xi^2} \right)^2 + \left(\frac{\partial^2 w_l}{\partial \eta^2} \right)^2 + 2 \left(\frac{\partial^2 w_l}{\partial \xi \partial \eta} \right)^2 \right] - K w_a^2 \right\} d\xi d\eta; \tag{39}
$$

$$
(\Pi_T)_{max} = \frac{\omega^2}{2} \int_0^1 \int_0^1 \left[\rho h \left(w_a^2 + w_l^2 \right) + \rho I \left(\left[\frac{\partial w_a}{\partial \xi} \right]^2 + \left[\frac{\partial w_a}{\partial \eta} \right]^2 + \left[\frac{\partial w_l}{\partial \xi} \right]^2 + \left[\frac{\partial w_l}{\partial \eta} \right]^2 \right) \right] d\xi d\eta. \tag{40}
$$

The Rayleigh solution procedure requires that the mid-plane deflections of the micro-panel be expressed in terms of an assumed mode shape function in the form

of a double Fourier series as:

$$w(\xi, \eta) = \sum_{m=1}^{M} \sum_{n=1}^{N} p_{mn} \phi_m(\xi) \beta_n(\eta), \tag{41}$$

such that p_{mn} is the amplitude of the function, while $\phi_m(\xi)$ and $\beta_n(\eta)$ are the mode functions that satisfy the Dirichlet boundary conditions of the micro-panel. The following comparison functions are used for the two boundary conditions considered in this study:

$$\begin{aligned} \text{SSSS:} \quad & w(\xi, \eta) = \sum_{m=1}^{M} \sum_{n=1}^{N} p_{mn} \sin(m\pi\xi) \sin(n\pi\eta); \\ & (m = 1, 2, 3\ldots; n = 1, 2, 3\ldots;) \end{aligned} \tag{42}$$

$$\text{CCCC:} \quad w(\xi, \eta) = \sum_{m=1}^{M} \sum_{n=1}^{N} p_{mn} \sin(m\pi\xi) \sin(\pi\xi) \sin(\pi\eta) \sin(n\pi\eta) \tag{43}$$

where m and n are the nodal lines in the ξ and η directions that determine the wave modes of the micro-panels. For the frequency values to be determined, the Rayleigh method minimizes the energy functional (by ensuring that $\partial \Pi / \partial p_{mn} = 0$) [Liu (2011)]. The minimization procedure results in a system of algebraic equations whose secular determinant yields the natural frequencies of the coupled system. In the next section, detailed numerical results are provided to evaluate the influence of different parameters of the model on the dynamic response of the coupled systems.

4 Special cases

Three different mechanistic cases of practical interests can be derived from the governing equation. These cases, shown in Fig. 3, are briefly highlighted below. For convenience, the following additional non-dimensional terms have been introduced in what follows:

$$\gamma = \zeta/h; \quad \alpha_{\text{eff}} = Ka^4/D; \quad \mu = h/a; \quad \lambda_{nm} = \omega_{nm} a^2 \sqrt{\rho h/D}; \tag{44}$$

4.1 Asynchronous motion of the coupled system

The case of the asynchronous motion of the coupled system, which is also referred to as the out-of-phase vibration, occurs when the two micro-panels move in different directions [Murmu and Adhikari (2011)]. In such case the condition of motion stipulates that $w_a \neq 0$. Under this condition, the Rayleigh method yields an upper

estimate of the frequency of the coupled micro-panels with the SSSS edge conditions as:

$$
(\lambda_{nm})^2 =
$$
$$
\left[\frac{12\gamma^2\left(-6m^4\pi^4+6m^4\pi^4v - 12m^2n^2\pi^4\phi^2+12m^2n^2\pi^4v\phi^2 - 6n^4\pi^4\phi^4 + 6n^4\pi^4v\phi^4\right)}{12 + \mu^2\phi + \mu^2\phi^3} \right.
$$
$$
\left. + \frac{12\left(m^4\pi^4 + 2m^2n^2\pi^4\phi^2 + n^4\pi^4\phi^4 + 2\alpha_{eff}\right)}{12 + \mu^2\phi + \mu^2\phi^3} \right].
$$

(45)

In Eq. (45), γ now represents the influence of the size-effect (that is, the material length scale of the micro-panel). This specific parameter quantifies the size-dependent vibration dynamics of the micro-panel with respect to the micro-panel's thickness. Also, α_{eff} is the non-dimensional averaged stiffness of the elastic connections, while μ and ϕ represent the thickness-to-length ratio and the aspect ratio of the micro-panel, respectively

4.2 Synchronous motion of the coupled system

Under a synchronous motion, the movements of the two micro-panels are in sync. Hence, this case is also referred to as the in-phase vibration Here, the condition of motion during the in-phase vibration requires that $w_a = 0$. With this, the Rayleigh method again yields an upper estimate of the frequency of the coupled micro-panels with SSSS edge conditions as:

$$
(\lambda_{nm})^2 =
$$
$$
\left[\frac{12\left(m^4\pi^4 + 2m^2n^2\pi^4\phi^2 + n^4\pi^4\phi^4\right)}{12 + \mu^2\phi + \mu^2\phi^3} \right.
$$
$$
\left. + \frac{12\gamma^2\left(-6m^4\pi^4 + 6m^4\pi^4v - 12m^2n^2\pi^4\phi^2 + 12m^2n^2\pi^4v\phi^2 - 6n^4\pi^4v\phi^4\right)}{12 + \mu^2\phi + \mu^2\phi^3} \right].
$$

(46)

4.3 Motion of the upper-panel supported by the ribs

The third special case relates to the situation when the lower micro-panel is a rigid base. Such situations do arise in the development of a mass sensing device [Agache, Blanco-Gomez, Cochet and Caillat (2011)]. When this occurs, then $w_l = 0$. Consequently, the frequency of the remnant systems is governed by the geometric and material properties as well as the boundary conditions of the upper micro-panel and

the ribs. The upper estimate of the frequency of the remnant system with a SSSS edge conditions for the upper micro-panel then takes the simplified form:

$$(\lambda_{nm})^2 = \left[\frac{12\left(\pi^4\left(1+6\gamma^2\left(-1+\upsilon\right)\right)\left(m^2+n^2\varphi^2\right)^2 + \alpha_{eff}\right)}{12+\mu^2\left(\varphi+\varphi^3\right)} \right] \tag{47}$$
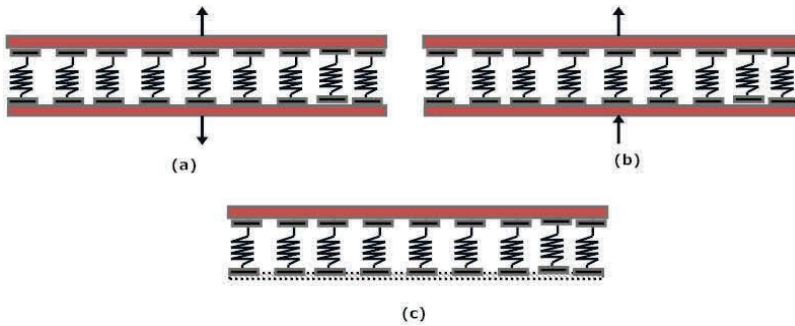
Figure 3: Special cases of the rib-connected micro-panels: (a) out-of-phase motion; (b) in-phase motion; and (c) motion of a single rib-supported micro-panel.

5   Discussion

The centerpiece of this section is to detail the qualitative and quantitative results relating to the free vibration properties of the system, based on the formulation presented in the foregoing sections. Principally, the section details the variation of the natural frequencies of the system with respect to changes in the aspect ratio (φ), the material length scale parameter (γ), the Poisson's ratio (υ), the thickness-to-span ratio (μ), and the stiffness of the ribs (α_{eff}). For the reported analyses, the effective material properties of the polymeric micro-panel are assumed to be: $E = 1.44GPa$; $\rho = 1220kg/m^3$; and $\nu = 0.38$. Furthermore, based on the experimental work of Lam, Yang, Chong, Wang and Tong (2003), the material length scale parameter for the epoxy micro-plate is restricted to a conservative value of $\zeta = 17.6\mu m$. Meanwhile, for polymeric structural elements with underlying polymer chains of finite stiffness, the material length scale parameter (ζ) is reported to be directly related to the effective averaged Frank elastic constant [Gao, Huang and Reddy (2013)]. For the analyses that follow, the thickness values considered is in the range $20\mu m \leq h \leq 176\mu m$. Besides, each rib is idealized as a fixed-fixed bar. Thus for each rib, the equivalent stiffness is estimated from $k_r = 192E_rI_r/L_r^3$, where

A_r, I_r, E_r, and L_r are the cross-sectional area, the moment of inertia, the Young's modulus and length of each rib.

5.1   *Validation*

For the purpose of validation, the governing equation of the system is modified by eliminating the parameters μ, α_{eff} and γ from the mathematical model. With this elimination, the governing equation is reduced to that of the Kirchhoff's plate theory [Szilard (2004)]. Tab. 1 reveals the comparison of the frequency values, based on the reduced form of the current model, with the classic work of Leissa (1973). Tab. 1 contains selected numerical results for a panel (treated as a plate) under the SSSS edge conditions and the CCCC edge conditions.

Tab. 2 provides the validation of the non-dimensional frequencies of a micro-plate with simply-supported edges. The governing equation employed for the results in Tab. 2 contains γ, but it does not contain α_{eff} and μ. The validation involves comparison with the closed-form expression presented in Yin, Qian, Wang and Xia (2010). It is noticed from Tab. 2 that a good agreement is achieved between the predicted non-dimensional frequency from the current method and the closed-form solution.

For brevity sake, the discussion is restricted to the two lowest symmetrical modes of the flexural vibration (whose non-dimensional frequency parameters are λ_{11} and λ_{22}) in the next subsections. For completeness, the mode shapes corresponding to both λ_{11} and λ_{22} are shown in Figs 4 and 5, respectively. In these figures, the contour plot corresponding to each of the two vibration modes are also provided under each of the mode shape. From the plots, it is noticed that increasing values of the small-scale parameter stiffen the response of the micro-panel. Besides, as seen from the contour plots, higher values of the small-scale parameter generate more equilibrium positions during the deformation of the system.

5.2   *Frequency distribution and frequency shift*

To evaluate the frequency shift induced by the small-scale parameter, a percentage change in the computed natural frequencies based on the MCST and the classical (size-independent) theory is defined as:

$$R_{nm} = \left| \frac{(\lambda_{nm})_{CCT} - (\lambda_{nm})_{MCST}}{(\lambda_{nm})_{CCT}} \right| \times 100 \tag{48}$$

where $(\lambda_{nm})_{MCST}$ is the natural frequency of the system from the MCST, while $(\lambda_{nm})_{CCT}$ is the corresponding natural frequency from the CCT. Besides, λ_{nm} is the non-dimensional natural frequency parameter defined as:

$$\lambda_{nm} = \omega_{nm} a^2 \sqrt{\rho h / D}. \tag{49}$$

Table 1: Validation of the non-dimensional frequencies of a classical plate.

Normalized Natural Frequency (λ) ($\mu = 0, \alpha_{eff} = 0, \gamma = 0$)					
CCCC					
φ	Method	λ_{11}	λ_{12}	λ_{21}	λ_{22}
2/3	Present	27.853	43.424	68.364	83.351
	Analytical [Leissa (1973)]	27.010	41.716	66.148	79.850
1.0	Present	37.221	70.081	76.231	113.390
	Analytical [Leissa (1973)]	35.992	70.123	73.413	108.27
1.5	Present	62.680	153.810	97.704	187.532
	Analytical [Leissa (1973)]	60.772	148.820	93.860	179.66
SSSS					
2/3	Present	14.256	27.415	43.864	57.024
	Analytical [Leissa (1973)]	14.256	27.416	43.865	57.024
1.0	Present	19.739	49.348	49.348	78.956
	Analytical [Leissa (1973)]	19.739	49.348	49.348	78.957
1.5	Present	32.076	98.69	61.685	128.305
	Analytical [Leissa (1973)]	32.076	98.696	61.685	128.305

Table 2: Validation of the non-dimensional frequencies of a micro-plate with simply-supported edges.

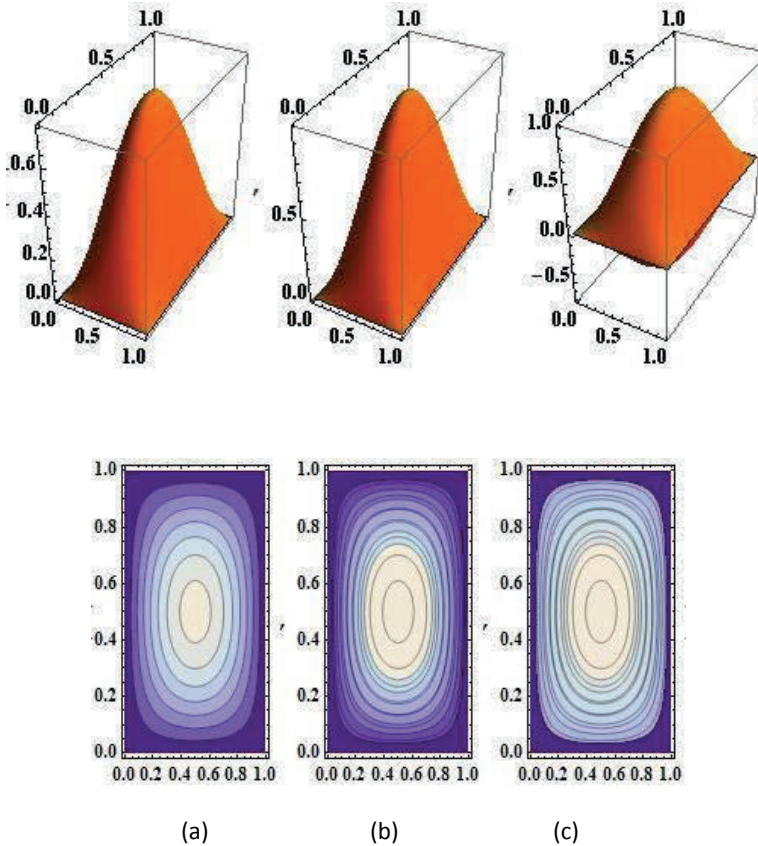| Normalized Natural Frequency (λ) ($\mu = 0, \alpha_{eff} = 0, \upsilon = 0.38$)						
	$\gamma = 0.2$		$\gamma = 0.5$		$\gamma = 0.8$	
φ	Rayleigh Method	[Yin, Qian, Wang and Xia (2010)]	Rayleigh Method	[Yin, Qian, Wang and Xia (2010)]	Rayleigh Method	[Yin, Qian, Wang and Xia (2010)]
2/3	15.28	15.28	19.81	19.81	26.22	26.22
1.0	21.16	21.16	27.42	27.42	36.29	36.29
1.5	34.38	34.38	44.56	44.56	58.97	58.97

Figure 4: The variation in the mode shape along with the corresponding contour plots of the lowest symmetrical mode (λ_{11}): (a) $\gamma = 0$; (b) $\gamma = 0.2$; and (c) $\gamma = 0.8$.

Summarized in Figs 68 are the distributions of the frequency variations for the three mechanistic cases of the coupled systems highlighted in section 4. Precisely, illustrated in Figs 6(a) and 6(b) are the distributions of the natural frequencies for the first symmetric vibration mode, under the SSSS and the CCCC boundary conditions, respectively. In each of the plot, the dummy variables $C1, C2$ and $C3$ refer to case 1, case 2 and case 3, respectively. It is recalled that case 1 relates to the out-of-phase motion of the coupled micro-panels, case 2 refers to the in-phase vibration of the coupled micro-panels, and case 3 is the motion of a single rib-supported micro-panel (case 3). Fig. 7 is indicative of the distribution of the natural frequencies for the second symmetric vibration modes of the three mechanistic cases. It is noticed from Fig. 7 that the frequency response increases with the aspect ratio (similar
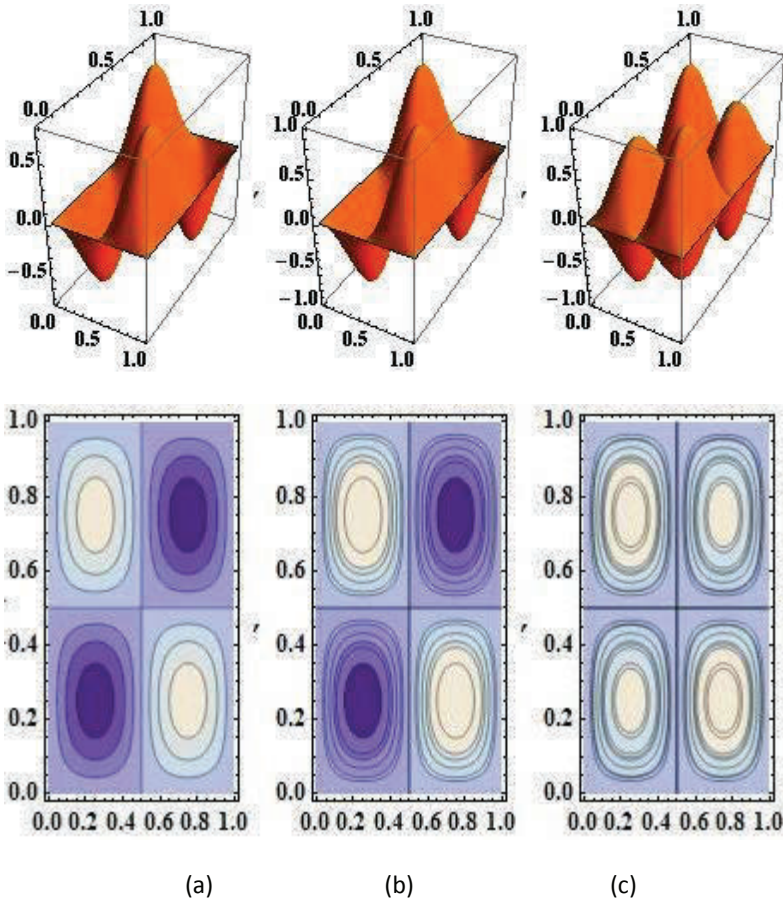
Figure 5: The variation in the mode shape and the contour plots of the second symmetrical mode (λ_{22}): (a) $\gamma = 0$; (b) $\gamma = 0.2$; and (c) $\gamma = 0.8$.

to Fig. 6). While a clear pattern of skew-symmetric distribution of the frequency values is easily noticed in Figs 6 and 7, a number of additional subtle observations can be made from the plots. First, in Fig. 6a, the lowest non-dimensional natural frequency value for the out-of-phase motion $(C1)$ is more than the highest non-dimensional natural frequency value for the other two cases for the aspect ratio of 0.2. However, under an increased value of the aspect ratio, the difference in the natural frequency values for the three cases approaches each other, although $C1$ still maintains the lead. Furthermore, in Fig. 6(b), the difference in the degrees of influence of the aspect ratio and the small-scale parameter on the pattern of the frequency increase is found to be comparatively similar across the three cases.
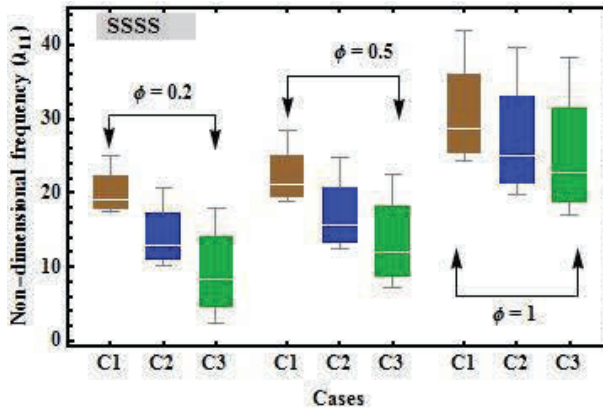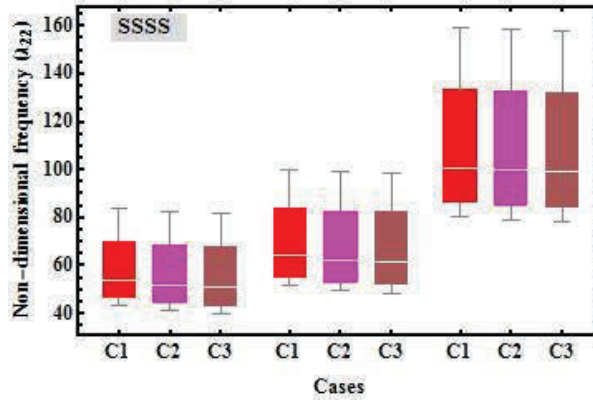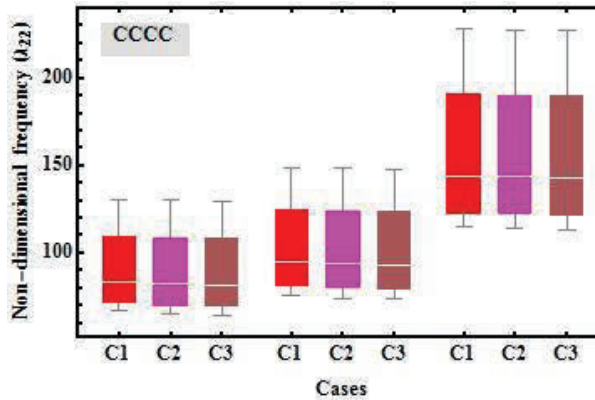
(a)
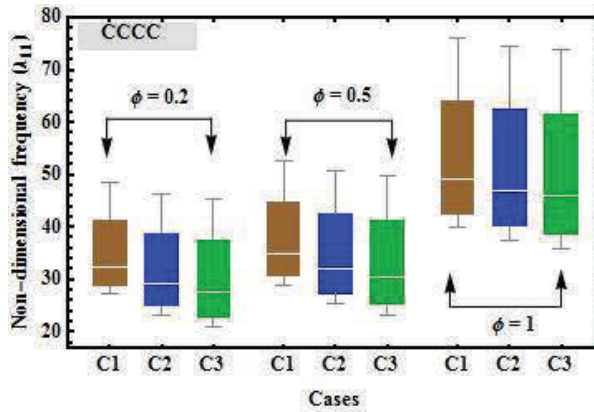
(b)

Figure 6: Distribution of the natural frequencies for the first symmetric vibration modes of the systems: (a) under four simply supported edges; (b) under fully clamped edges.

Fig. 8 represents a visual display of the boundary condition under which the effect of the small-scale parameter exerts a greater influence. From this plot, it is seen that the CCCC edge condition is more heavily affected by the size-effect than the SSSS edge condition for the two vibration modes. It is worth pointing out that, since the CCCC edge conditions do naturally yield greater frequency response, normalized frequency values are employed for Fig. 8. Still, it is noticed that the effect of the small-scale parameter is more pronounced on the frequency of the system under

(a)

(b)

Figure 7: Distribution of the natural frequencies for the second symmetric vibration modes ($\alpha_{eff} = 100$): (a) micro-panels with four simply supported edges; (b) micro-panels with fully clamped edges.

the CCCC edge condition.

Additional plots to examine the effects of the geometric and small-scale parameters are provided in Figs 9-12, all of which are related to the system with the SSSS edge conditions. It is observed from Fig. 9(a) that as the micro-panel's thickness reduces, up to 20% increase in the frequency value is attainable for an aspect ratio of 1 (basically a square micro-panel). On the other hand, Fig. 9(b) illustrates the vanishing influence of the size-effect on the natural frequency value of the panels
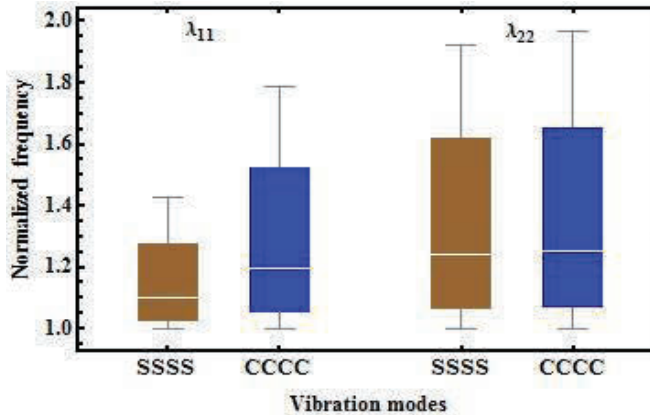
Figure 8: A comparison of the effect of the small-scale parameter on the out-of-phase motion of the coupled system.

as the thickness increases.

Fig. 10 shows the differential trend of the influence of the small-scale effect on the responses of the three mechanistic cases of the coupled system. From this plot, one is able to conclude that the out-of-phase motion of the coupled system experiences the most softening effect arising from the decreasing value of the micro-panels' thickness. Demonstrated in Fig. 11 is the inverse relationship between the frequency response of the out-of-phase motion of the coupled system with the thickness-to-span ratio (μ).

In Fig. 12, the influence of the ribs' effective stiffness on the three special cases is shown. Specifically, Fig. 12(a) reveals the trend of the frequency increase when the ribs' effective stiffness parameter approaches zero, while Fig. 12(b) shows difference in the trend for the three cases when the ribs' effective stiffness parameter is maintained at a modest value of 100.

5.3 *Identification of the order of influence of the model's parameters*

The results presented under subsection 5.3 are generated by the traditional method of analysis, where one varies a single parameter of the model while keeping all others constant. Essentially, this method is analogous to the so called *one factor-at-a-time* (OFAT) analysis [Karray and Silva (2004)]. One of the drawbacks of the OFAT methodology in the traditional computational mechanics is the inherent underestimation of the possibility of interaction effects between the variables that influence the response of the system under consideration. In the present study for
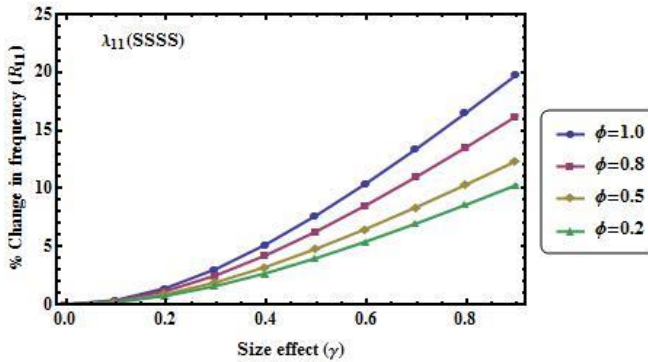
(a)
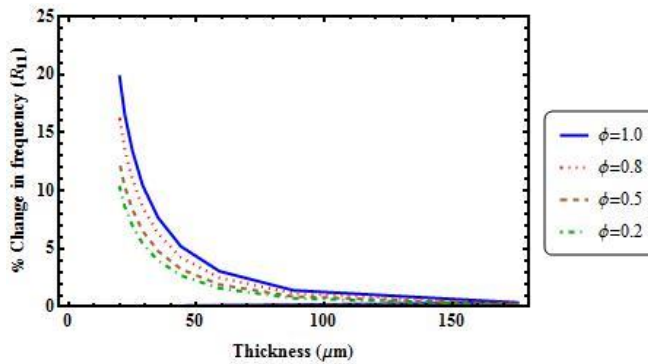
(b)

Figure 9: The quantification of the percentage change in frequency values: (a) the change in frequency against the small-scale effect; (b) the change in frequency against the micro-panels' thickness.

instance, we recognized five continuous numerical dimensionless parameters that could influence the response of the system as seen in Fig. 13. These five continuous numerical parameters (or factors) are the aspect ratio (φ), the small-scale parameter (γ), the ribs' effective stiffness (α_{eff}), the Poisson's ratio (ν) and the thickness-to-span ratio (μ). In what follows, the OFAT analysis is complemented with the applied statistical method of design of experiment (DOE) [Dean and Voss (1999); Mustapha and Zhong (2012)] to examine the order of influence of these parameters.

Figs. 14-16 are indicative of the outcome of the analyses based on the use of the DOE. Two levels of each of the five parameters are considered for the numerical
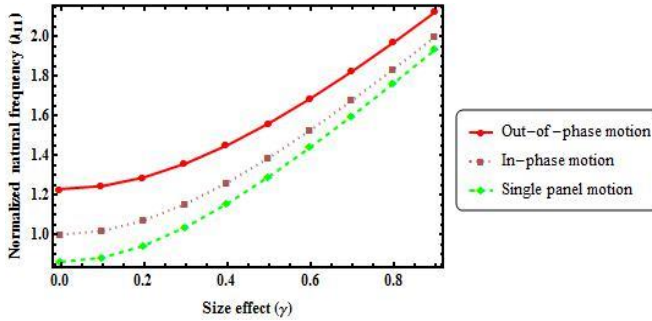
Figure 10: Variation of frequency values with varying value of the material length scale for the special motion types of the system.
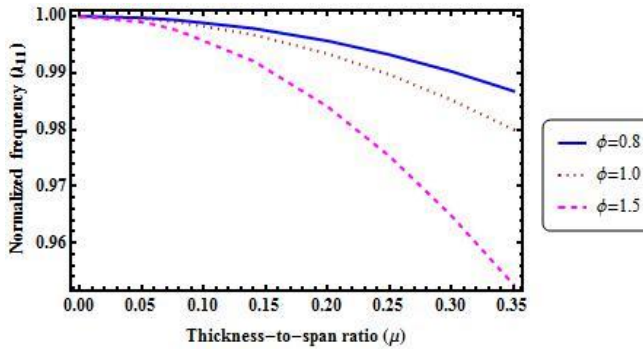

Figure 11: The effect of rotary inertia on the two lowest symmetric vibration modes for the out-of-phase motion of the coupled system.

DOE. Based on the established procedure of DOE, an experimental design involving five input factors at two levels (low and high) becomes a problem of 2^p number of experimental runs, where the superscript p is the number of factors. The capability of the statistical software Minitab [Lesik (2010)] is used to run a randomized design of the experiment. It is pointed out that the term experiment is used in the sense of numerical analysis experiment in the current setting. The values of the factors at each run of the experiment are presented in Tab. 3.

The ordered ranking of the model's factors (also refers to as main effects) as they influence the response of the system are presented in the form of the Pareto charts depicted in Figs 14-16. In these charts the terms A, B, C, D and E are dummy variables that symbolize the ribs effective stiffness, the aspect ratio, the size-effect, the thickness-to-span ratio and the Poisson's ratio, respectively. The combinations of
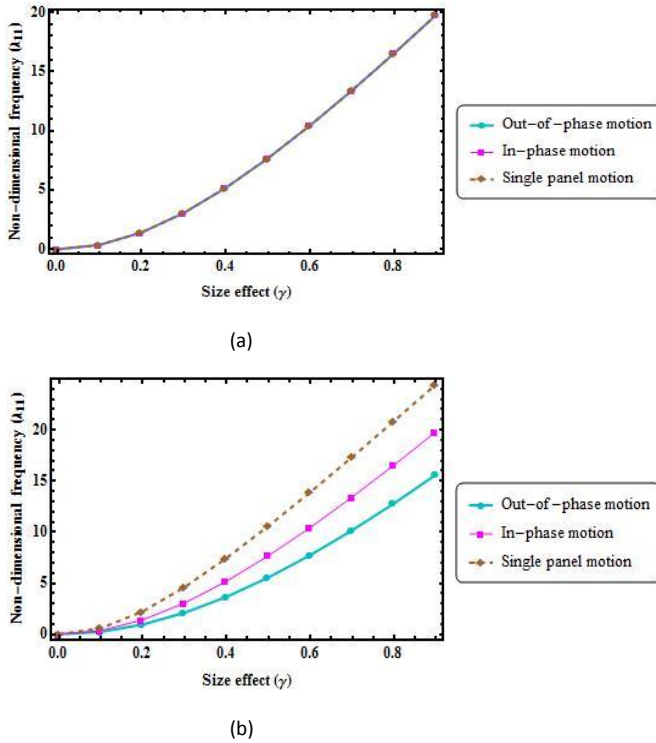
(a)

(b)

Figure 12: The effect of the ribs' stiffness on the three special cases: (a) a negligible ribs' effective stiffness parameter; (b) ribs' effective stiffness maintained at 100.
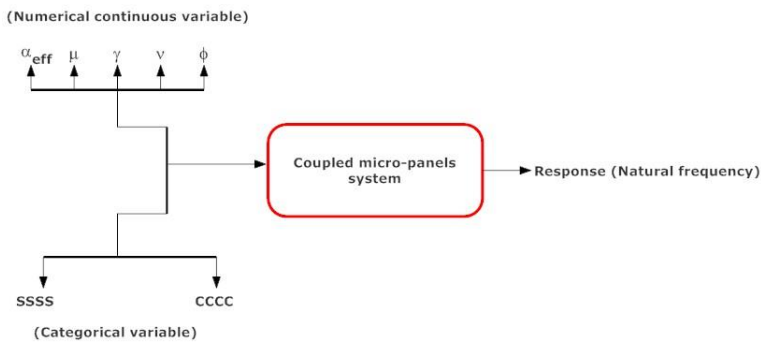

Figure 13: The relation between the inputs and the output of the coupled micro-panels system.

these dummy variables (such as *AB*, *AC* and *ABC* etc.,) are visible in these charts, and they are called the interaction effects. Specifically, Figs. 14, 15 and 16 represent the Pareto chart of case 1 (the asynchronous motion), case 2 (the synchronous motion) and case 3 (the motion of a rib-connected micro-panel), respectively.

It is observed from Figs 14-16 that the factor that affects the natural frequency of the motion of the three cases the most is the interaction factor *BC*. This interaction factor is created by the interaction between the aspect ratio and the size-effect parameter. Furthermore, it is observed from the Pareto charts that the Poisson's ratio has a somewhat negligible effect on the motion of the three systems. However, the interaction effect created between the Poisson's ratio, the aspect ratio and size-effect (*BCE*) is the fourth most significant factor that influences the behavior of the synchronous motion. An additional conclusion that can be drawn from these charts is the fact the size-effect is the second most significant factor that alters the natural frequency of the system for case 1 and case 2. It is also the third most significant factor for case 3. Besides, the thickness-to-span ratio is discovered not to significantly affect the response of any of the three mechanistic cases.
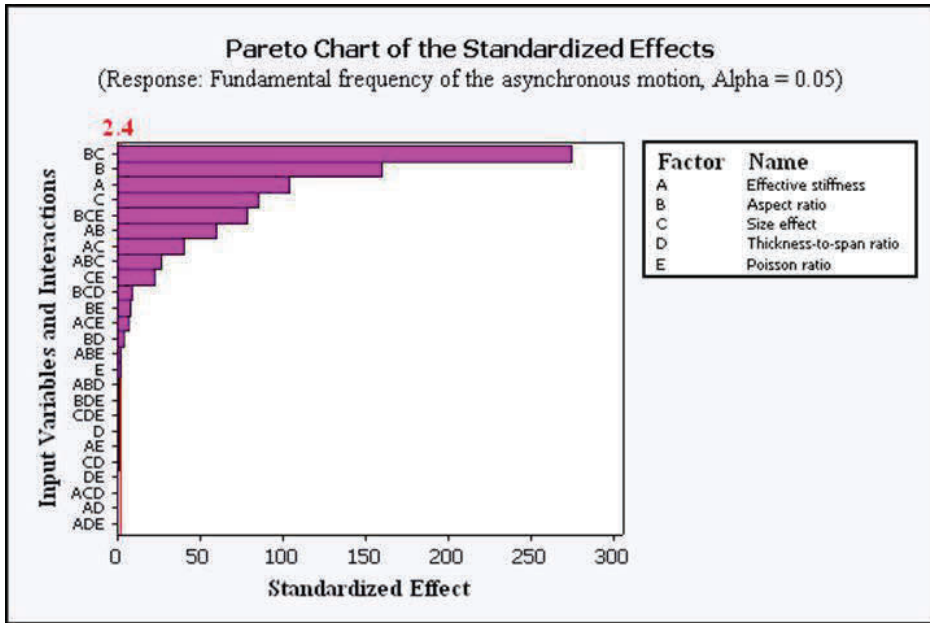

Figure 14: The Pareto chart of the ordered ranking of the model's factors for the asynchronous motion of coupled system.

Table 3: Randomized numerical experimental runs.

|	Continuous input variables					Response (λ_{11})		
						Case 1	**Case 2**	**Case 3**
1	10	1.5	0.8	0.05	0.25	63.308	63.150	63.071
2	200	0.1	0.8	0.25	0.38	27.121	18.323	11.656
3	200	0.1	0.8	0.25	0.25	28.020	19.630	13.617
4	200	0.1	0.1	0.25	0.25	22.440	10.187	9.803
5	10	1.5	0.1	0.25	0.25	32.681	32.381	32.230
6	10	1.5	0.1	0.05	0.38	32.955	32.650	32.497
7	10	0.1	0.1	0.25	0.25	11.125	10.187	9.684
8	10	1.5	0.1	0.05	0.25	33.076	32.773	32.620
9	10	0.1	0.1	0.25	0.38	11.090	10.149	9.644
10	10	0.1	0.8	0.05	0.25	20.137	19.635	19.378
11	10	0.1	0.8	0.25	0.38	18.861	18.323	18.049
12	200	1.5	0.8	0.25	0.38	61.501	58.243	56.544
13	10	1.5	0.1	0.25	0.38	32.561	32.260	32.108
14	200	1.5	0.1	0.25	0.25	37.929	32.381	29.214
15	200	0.1	0.1	0.25	0.38	22.423	10.149	9.843
16	10	0.1	0.8	0.25	0.25	20.132	19.630	19.373
17	10	0.1	0.1	0.05	0.38	11.093	10.151	9.646
18	200	1.5	0.1	0.05	0.38	38.284	32.650	29.432
19	200	0.1	0.8	0.05	0.25	28.027	19.635	13.621
20	10	0.1	0.1	0.05	0.25	11.128	10.190	9.686
21	200	1.5	0.8	0.25	0.25	65.440	62.395	60.812
22	200	1.5	0.8	..	0.38	62.245	58.948	57.228
23	200	1.5	0.1	0.05	0.25	38.388	32.773	29.568
24	200	1.5	0.1	0.25	0.38	37.826	32.260	29.080
25	10	1.5	0.8	0.05	0.38	59.117	58.948	58.863
26	10	0.1	0.8	0.05	0.38	18.866	18.328	18.053
27	10	1.5	0.8	0.25	0.38	58.410	58.243	58.159
28	200	0.1	0.1	0.05	0.25	22.446	10.190	9.806
29	200	1.5	0.8	0.05	0.25	66.239	63.150	61.548
30	10	1.5	0.8	0.25	0.25	62.551	62.395	62.317
31	200	0.1	0.8	0.05	0.38	27.127	18.328	11.659
32	200	0.1	0.1	0.05	0.38	22.428	10.151	9.846
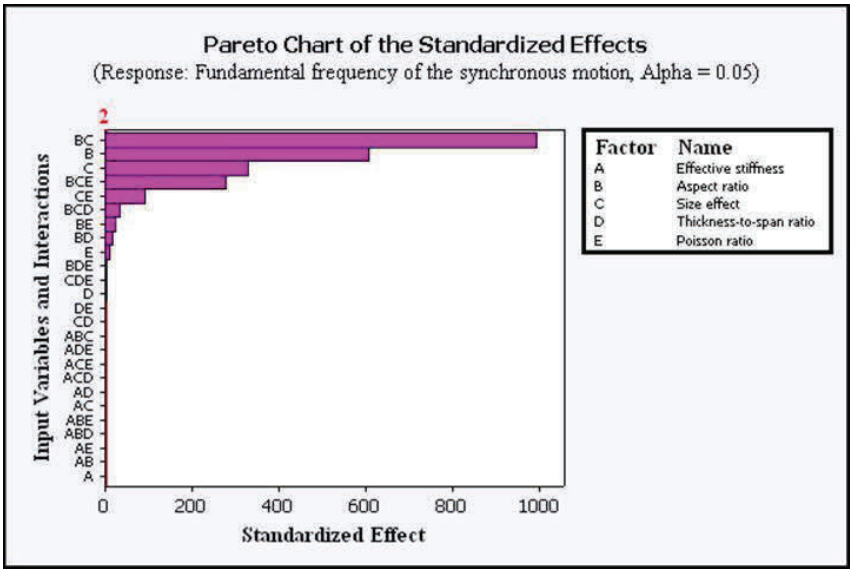
Figure 15: The Pareto chart of the ordered ranking of the model's factors for the synchronous motion of coupled system.
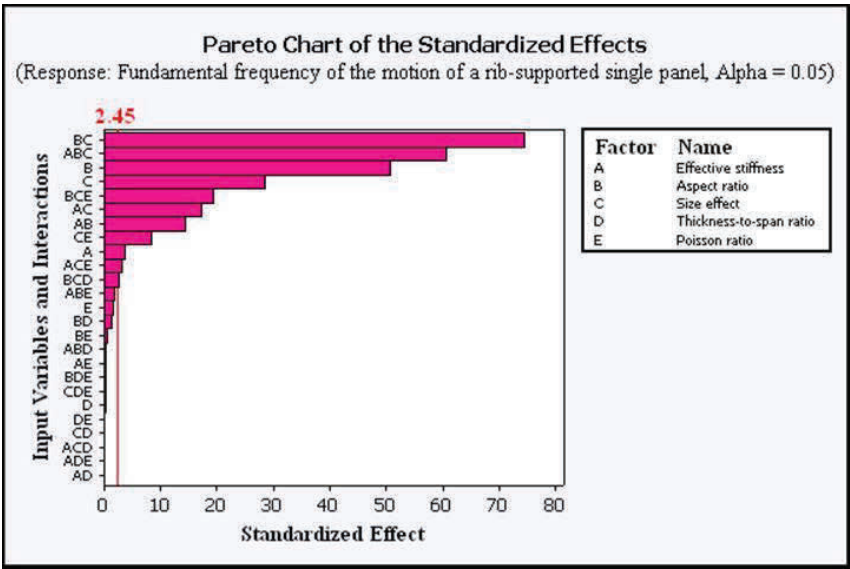

Figure 16: The Pareto chart for the motion of ribs-supported single micro-panel.

6 Conclusion

On the basis of the extended Hamilton's principle and the modified couple stress theory, the governing equations of a rib-connected system of coupled micro-panels are derived. Starting from a displacement trial field, the derivation considers the deformation of a single micro-panel embedded in a Euclidean 3-space $\forall$. The derivation procedure yields three field equations. Two of the field equations represent the extensional vibration mode of the micro-panel, while the third equation relates to the flexural vibration mode. Given the focus of the current study, the third field equation, which accounts for the flexural vibration of the micro-panel and is uncoupled from the extensional modes is adopted for comprehensive response analyses.

In analyzing the behavior of the coupled micro-scale panels, three forms of special cases of motion of the system were assessed: (i) the out-of-phase motion; (ii) the in-phase motion; and (iii) the motion of a single micro-panel with rib connections and a rigid base. The vibration characteristics under each of these motion types were studied systematically for the determination of the frequency shift and the pattern of the frequency distribution. The study reaffirms the expected substantial increase in natural frequency value for a lower range of the micro-panel's thickness. A skew-symmetric pattern of distribution of the shift in natural frequencies values is discovered for the first and second symmetric modes of the coupled system under the two edge conditions studied. Furthermore, it is noticed that, for lower values of the aspect ratio, the lowest non-dimensional natural frequency value for the out-of-phase motion is more than the highest non-dimensional natural frequency value for both the in-phase motion and the motion of a single micro-panel with rib connection. It is also found that the effect of the material length scale on the frequency of the out-of-phase motion is higher when the edges are fully clamped than when simply-supported. Through Pareto analysis, notable interaction effects were discovered between the models' parameters.

Although extrapolating theoretical conclusions to experimental studies do come with certain challenges, preliminary theoretical investigations such as the one carried out in this study strives to provide a cogent basis for close scrutiny of future experimental results. The observations from this study are expected to pave the way for the recognition of key variables (main effects or interactions effects) that might be employed in the future optimization of the system's geometry and response.

References

Agache, V.; Blanco-Gomez, G.; Cochet, M.; Caillat, P. (2011): *Suspended nanochannel in MEMS plate resonator for mass sensing in liquid*. Micro Electro Mechanical Systems (MEMS), 2011 IEEE 24th International Conference on.

Aifantis, E. C. (1992): On the role of gradients in the localization of deformation and fracture. *International Journal of Engineering Science*, vol. 30, no. 10, pp. 1279-1299.

Aifantis, E. C. (2011): On the gradient approach – Relation to Eringen's nonlocal theory. *International Journal of Engineering Science*, vol. 49, no. 12, pp. 1367-1377.

Akgöz, B.; Civalek, Ö. (2013): Free vibration analysis of axially functionally graded tapered Bernoulli-Euler microbeams based on the modified couple stress theory. *Composite Structures*, vol. 98, pp. 314-322.

Akgöz, B.; Civalek, Ö. (2013): Modeling and analysis of micro-sized plates resting on elastic medium using the modified couple stress theory. *Meccanica*, vol. 48, no. 4, pp. 863-873.

Anthoine, A. (2000): Effect of couple-stresses on the elastic bending of beams. *International Journal of Solids and Structures*, vol. 37, no. 7, pp. 1003-1018.

Ardito, R.; Baldasarre, L.; Corigliano, A.; De Masi, B.; Frangi, A.; Magagnin, L. (2013): Experimental evaluation and numerical modeling of adhesion phenomena in polysilicon MEMS. *Meccanica*, vol. 48, no. 8, pp. 1835-1844.

Benkhelifa, E.; Farnsworth, M.; Tiwari, A.; Bandi, G. (2010): Design and optimisation of microelectromechanical systems: a review of the state-of-the-art. *International Journal of Design Engineering*, vol. 3, no. 1, pp. 41-76.

Boisen, A.; Dohn, S.; Keller, S. S.; Schmid, S.; Tenje, M. (2011): Cantilever-like micromechanical sensors. *Reports on Progress in Physics*, vol. 74, no. 3.

Chiroiu, V.; Munteanu, L.; Delsanto, P. P. (2010): Evaluation of the Toupin-Mindlin theory for predicting the size effects in the buckling of the carbon nanotubes. *Computers, Materials & Continua (CMC)*, vol. 16, no. 2, pp. 75.

Chiroiu, V.; Munteanu, L.; Gliozzi, A. S. (2010): Application of Cosserat Theory to the Modelling of Reinforced Carbon Nananotube Beams. *Computers Materials and Continua*, vol. 19, no. 1, pp. 1.

Cosserat, E.; Cosserat, F. (1909): Théorie des Corps Déformables. *A. Hermann et Fils, Paris*.

Dean, A. M.; Voss, D. (1999): *Design and analysis of experiments*, Springer.

Eringen, A. C. (1972): Nonlocal polar elastic continua. *International Journal of*

Engineering Science, vol. 10, no. 1, pp. 1-16.

Eringen, A. C.; Edelen, D. G. B. (1972): On nonlocal elasticity. *International Journal of Engineering Science*, vol. 10, no. 3, pp. 233-248.

Farokhi, H.; Ghayesh, M. H.; Amabili, M. (2013): Nonlinear dynamics of a geometrically imperfect microbeam based on the modified couple stress theory. *International Journal of Engineering Science*, vol. 68, pp. 11-23.

Fleck, N. A.; Hutchinson, J. W. (1993): A phenomenological theory for strain gradient effects in plasticity. *Journal of the Mechanics and Physics of Solids*, vol. 41, no. 12, pp. 1825-1857.

Fotouhi, M. M.; Firouz-Abadi, R. D.; Haddadpour, H. (2013): Free vibration analysis of nanocones embedded in an elastic medium using a nonlocal continuum shell model. *International Journal of Engineering Science*, vol. 64, pp. 14-22.

Gao, X. L.; Huang, J. X.; Reddy, J. N. (2013): A non-classical third-order shear deformation plate model based on a modified couple stress theory. *Acta Mechanica*, vol. 224, no. 11, pp. 2699-2718.

Georgiadis, H. G.; Velgaki, E. G. (2003): High-frequency Rayleigh waves in materials with micro-structure and couple-stress effects. *International Journal of Solids and Structures*, vol. 40, no. 10, pp. 2501-2520.

Güven, U. (2011): The investigation of the nonlocal longitudinal stress waves with modified couple stress theory. *Acta Mechanica,* vol. 221, no. 3-4, pp. 321-325.

Jomehzadeh, E.; Noori, H. R.; Saidi, A. R. (2011): The size-dependent vibration analysis of micro-plates based on a modified couple stress theory. *Physica E: Low-dimensional Systems and Nanostructures*, vol. 43, no. 4, pp. 877-883.

Karray, F.; Silva, C. D. (2004): Soft Computing and Tools of Intelligent Systems Design: Theory and Applications.

Kun, W.; Nguyen, C. T. C. (1999): High-order medium frequency micromechanical electronic filters. *Microelectromechanical Systems, Journal of*, vol. 8, no. 4, pp. 534-556.

Lam, D. C. C.; Yang, F.; Chong, A. C. M.; Wang, J.; Tong, P. (2003): Experiments and theory in strain gradient elasticity. *Journal of the Mechanics and Physics of Solids,* vol. 51, no. 8, pp. 1477-1508.

Leissa, A. W. (1973): The free vibration of rectangular plates. *Journal of Sound and Vibration*, vol. 31, no. 3, pp. 257-293.

Lesik, S. A. (2010): *Applied Statistical Inference with MINITAB*, CRC Press.

Liew, K. M.; Wong, C. H.; He, X. Q.; Tan, M. J.; Meguid, S. A. (2004): Nanomechanics of single and multiwalled carbon nanotubes. *Physical Review B*

- Condensed Matter and Materials Physics, vol. 69, no. 11, pp. 1154291-1154298.

Liu, D.-S.; Tu, C.-Y.; Chung, C.-L. (2012): Eigenvalue Analysis of MEMS Components with Multi-defect using Infinite Element Method Algorithm. *Computers Materials and Continua*, vol. 28, no. 2, pp. 97.

Liu, M. (2011): Orthogonal Tapered Beam Functions in the Study of Free Vibrations for Non-uniform Isotropic Rectangular Plates. *Computers Materials and Continua*, vol. 22, no. 2, pp. 97.

Mahdavi, M. H.; Farshidianfar, A.; Tahani, M.; Mahdavi, S.; Dalir, H. (2008): A more comprehensive modeling of atomic force microscope cantilever. *Ultramicroscopy*, vol. 109, no. 1, pp. 54-60.

Manzaneque, T.; Ruiz, V.; Hernando-Garcia, J.; Ababneh, A.; Seidel, H.; Sanchez-Rojas, J. L. (2012): Characterization and simulation of the first extensional mode of rectangular micro-plates in liquid media. *Applied Physics Letters* **101**(15): 151904-151904-151904.

Marin, M.; Agarwal, R. P.; Othman, M. (2014): Localization in Time of Solutions for Thermoelastic Micropolar Materials with Voids. *CMC: Computers, Materials & Continua*, vol. 40, no. 1, pp. 35-48.

Mattila, T.; Kiihamäki, J.; Lamminmäki, T.; Jaakkola, O.; Rantakari, P.; Oja, A.; Seppä, H.; Kattelus, H.; Tittonen, I. (2002): A 12 MHz micromechanical bulk acoustic mode oscillator. *Sensors and Actuators A: Physical*, vol. 101, no. 1–2, pp. 1-9.

Murmu, T.; Adhikari, S. (2011): Nonlocal vibration of bonded double-nanoplate-systems. *Composites Part B: Engineering*, vol. 42, no. 7, pp. 1901-1911.

Mustapha, K. B. (2014): Modeling of a functionally graded micro-ring segment for the analysis of coupled extensional–flexural waves. *Composite Structures*, vol. 117, pp. 274-287.

Mustapha, K. B.; Zhong, Z. W. (2012): A new modeling approach for the dynamics of a micro end mill in high-speed micro-cutting. *Journal of Vibration and Control*.

Mustapha, K. B.; Zhong, Z. W. (2012): Spectral element analysis of a non-classical model of a spinning micro beam embedded in an elastic medium. *Mechanism and Machine Theory*, vol. 53, pp. 66-85.

Mustapha, K. B.; Z. W. Zhong (2012): Wave propagation characteristics of a twisted micro scale beam. *International Journal of Engineering Science*, vol. 53, pp. 46-57.

Nguyen, C. T. C. (1995): *Micromechanical resonators for oscillators and filters*. Ultrasonics Symposium, 1995. Proceedings., 1995 IEEE.

Papacharalampopoulos, A.; Karlis, G.; Charalambopoulos, A.; Polyzos, D. (2010): BEM Solutions for 2 D and 3 D Dynamic Problems in Mindlin's Strain Gradient Theory of Elasticity. *Computer Modeling in Engineering & Sciences(CMES)*, vol. 58, no. 1, pp. 45-74.

Papargyri-Beskou, S.; Tsepoura, K. G.; Polyzos, D.; Beskos, D. E. (2003): Bending and stability analysis of gradient elastic beams. *International Journal of Solids and Structures*, vol. 40, no. 2, pp. 385-400.

Park, S. K.; Gao, X. L. (2006): Bernoulli-Euler beam model based on a modified couple stress theory. *Journal of Micromechanics and Microengineering*, vol. 16, no. 11, pp. 2355-2359.

Peddieson, J.; Buchanan, G. R.; McNitt, R. P. (2003): Application of nonlocal continuum models to nanotechnology. *International Journal of Engineering Science*, vol. 41, no. 3-5, pp. 305-312.

Reddy, J. N. (2002): *Energy principles and variational methods in applied mechanics*. Hoboken, N.J., Wiley.

Reddy, J. N. (2011): Microstructure-dependent couple stress theories of functionally graded beams. *Journal of the Mechanics and Physics of Solids*, vol. 59, no. 11, pp. 2382-2399.

Romanoff, J.; Reddy, J. (2014): Experimental validation of the modified couple stress Timoshenko beam theory for web-core sandwich panels. *Composite Structures*, vol. 111, pp. 130-137.

Sakhaee-Pour, A.; Ahmadian, M.; Vafai, A. (2008): Applications of single-layered graphene sheets as mass sensors and atomistic dust detectors. *Solid State Communications*, vol. 145, no. 4, pp. 168-172.

Szilard, R. (2004): *Theories and applications of plate analysis : classical, numerical, and engineering methods*. Hoboken, N.J., John Wiley.

Tang, Z.; Shen, S.; Atluri, S. (2003): Analysis of materials with strain-gradient effects: A meshless local Petrov-Galerkin (MLPG) approach, with nodal displacements only. *Computer Modeling in Engineering and Sciences*, vol. 4, no, 1, pp. 177-196.

Toupin, R. A. (1962): Elastic materials with couple-stresses. *Archive for Rational Mechanics and Analysis*, vol. 11, no. 1, pp. 385-414.

Uchic, M. D.; Dimiduk, D. M.; Florando, J. N.; Nix, W. D. (2004): Sample dimensions influence strength and crystal plasticity. *Science*, vol. 305, no. 5686, pp. 986-989.

Volkert, C. A.; Lilleodden, E. T. (2006): Size effects in the deformation of submicron Au columns. *Philosophical Magazine*, vol. 86, no. 33-35, pp. 5567-5579.

Wang, L.; Liu, H. T.; Ni, Q.; Wu, Y. (2013): Flexural vibrations of microscale pipes conveying fluid by considering the size effects of micro-flow and micro-structure. *International Journal of Engineering Science*, vol. 71, no. 0, pp. 92-101.

Xie, G.; Long, S. (2006): Elastic vibration behaviors oof carbon nanotubes based on micropolar mechanics. *CMC-TECH SCIENCE PRESS*-, vol. 4, no. 1, pp. 11.

Yang, F.; Chong, A. C. M.; Lam, D. C. C.; Tong, P. (2002): Couple stress based strain gradient theory for elasticity. *International Journal of Solids and Structures,* vol. 39, no. 10, pp. 2731-2743.

Yazdi, N.; Ayazi, F.; Najafi, K. (1998): Micromachined inertial sensors. *Proceedings of the IEEE*, vol. 86, no. 8, pp. 1640-1659.

Yin, L.; Qian, Q.; Wang, L.; Xia, W. (2010): Vibration analysis of microscale plates based on modified couple stress theory. *Acta Mechanica Solida Sinica*, vol. 23, no. 5, pp. 386-393.

Younis, M. I. (2011): MEMS Linear and Nonlinear Statics and Dynamics.